Zero electron kinetic energy spectroscopy of the $KrBr^-$, $XeBr^-$, and $KrCl^-$ anions

Ivan Yourshaw, Thomas Lenzer, Georg Reiser,[a] and Daniel M. Neumark
Department of Chemistry, University of California, Berkeley, California 94720
and Chemical Sciences Division, Lawrence Berkeley Laboratory, Berkeley, California 94720

(Received 22 April 1998; accepted 24 June 1998)

Three rare-gas halide (RgX^-) anions, $KrBr^-$, $XeBr^-$, and $KrCl^-$, and the corresponding neutral, open-shell van der Waals complexes are studied with anion zero electron kinetic energy spectroscopy. The spectra for each system reveal well-resolved progressions in the low frequency vibrations of the anion and one or more of the three neutral electronic states accessed by photodetachment, providing a detailed spectroscopic probe of the $Rg–X^-$ and Rg–X interaction potentials. In the case of $KrBr^-$, transitions to all three of the ''covalent'' neutral electronic states (the $X1/2$, $I3/2$, and $II1/2$ states) were observed. For $XeBr^-$, transitions to the $X1/2$ and $II1/2$ neutral states were observed. For $KrCl^-$, only the $X1/2$ state could be studied. From our data, we construct model potentials for the anion and each observed neutral state, and these are compared with other experimental and theoretical potentials. © *1998 American Institute of Physics.* [S0021-9606(98)01037-X]

I. INTRODUCTION

The characterization of the forces between weakly interacting species has attracted a great deal of experimental and theoretical attention in recent years. The interaction potentials between closed shell neutral species have been characterized in considerable detail as a result of this effort.[1,2] However, less is known about the interactions between open and closed shell atoms, or about those between ions and neutrals. In this work we describe new experimental results involving the latter two types of interactions. We report the results of studies of the rare gas–halide atom complexes $KrBr^-$, $XeBr^-$, and $KrCl^-$ using anion zero electron kinetic energy (ZEKE) spectroscopy. In these experiments we obtain spectroscopic information on both the neutral and negatively charged complex and derive accurate potentials for both the anion and neutral species. This work is a continuation of our earlier ZEKE studies of the $ArBr^-$, KrI^-, and ArI^- complexes,[3,4] and is part of an ongoing effort to obtain ZEKE spectra of the complete series of rare gas halides.

The rare gas halide (RgX^-) species are of interest because the $Rg–X^-$ interaction potentials determine the transport properties of halide ions in rare gases; these are important in understanding plasmas and gas discharges. Accurate interaction potentials are also crucial in studies of ion clusters of the type $X^-(Rg)_n$, which serve as protypical systems for understanding many-body effects in ion clusters.[4,5] Our spectra provide a direct spectroscopic probe of RgX^- anions. Prior to the work reported here, the only experimental results on the $KrBr^-$, $XeBr^-$, and $KrCl^-$ anions came from ion mobility studies,[6,7] from which potentials can be obtained by iterative fitting or direct inversion. Interaction potentials had also been derived within the framework of theoretical[8,9] and semiempirical[10–13] models. The equilibrium geometry and well depth of $XeBr^-$ have recently been calculated in a high level quantum chemistry calculation.[14]

The rare gas–halogen (RgX) complexes are important for their use in excimer lasers, in which lasing takes place between electronically excited, strongly bound charge transfer states and the repulsive wall of the weakly bound covalent ground states.[15] Excimer emission has also provided spectroscopic information on the charge transfer and covalent states. In the cases of KrBr and KrCl emission from the RgX charge transfer states to the ground state (the $B \rightarrow X$ band) is broad and relatively unstructured,[15] as is typical of bound-free transitions. However, recent emission studies of the $B \rightarrow X$ band in XeBr reveal extensive vibrational structure.[16,17] The covalent states of rare gas–halogen neutrals have also been probed in a series of scattering experiments. Information on the RgX species studied here comes from differential cross-section crossed molecular beam experiments of Lee and co-workers,[18] which yielded potentials for the KrBr and XeBr complexes, and from integral cross-section measurements by Aquilanti and co-workers,[19] who have characterized the potential of KrCl.

The neutral interactions are of interest also because they are simple examples of open shell–closed shell interactions. The effect of spin–orbit coupling on the rare gas–halogen interaction potentials has been discussed at length by Aquilanti and Haberland.[20,21] The two spin–orbit states of the ^2P halogen atom interact with the rare gas to give rise to three molecular electronic states. The lower $^2P_{3/2}$ state is split by the electrostatic interaction into two components, corresponding to $\Omega = 1/2$ (the $X1/2$ state, in the notation used here) and $\Omega = 3/2$ (the $I3/2$ state), where Ω is the projection of the total electronic angular momentum along the internuclear axis. The upper $^2P_{1/2}$ halogen state gives rise to the $II1/2(\Omega = 1/2)$ state in the complex.

[a]Current address: Agfa, Abt. FT-EO, Tegernseer Landstr. 161, 81534 Munich, Germany.

Anion ZEKE spectroscopy of rare gas halides probes the van der Waals well region of the covalent states; this complements earlier studies of emission from excimer states. Our experiments also complement the scattering experiments because, whereas the scattering cross-sections contain information about the *absolute* values of the bond length and well depths of the complexes, the ZEKE spectra are sensitive only to the *relative* differences between the anion and neutral potentials. However, in the ZEKE spectra one can observe vibrationally resolved photodetachment transitions to the various neutral electronic states, whereas in the crossed beam experiments the contributions of the $X1/2$ and $I3/2$ states to the experimental signal are not clearly separated and must be extracted by an appropriate data inversion procedure. Also, in the crossed beam experiments involving Br or I atoms, the $II1/2$ electronic state arising from the upper $^2P_{1/2}$ spin–orbit state of the halogen atom is generally not probed because the population of this state is negligible. In the ZEKE experiments, well-resolved spectra of the $II1/2$ states of the KrBr and XeBr systems are seen, and accurate potentials can be derived for these states for the first time.

The anion potentials derived here are a significant improvement over previously available potentials. While our ground state potentials for KrBr and XeBr are essentially the same as those derived from scattering and excimer emission experiments, our excited states potentials represent improvements over previous work, particularly for the $II1/2$ state. In the case of KrCl, our spectra confirm the neutral potentials previously deduced from the scattering experiments.

This article is organized as follows: In Sec. II we describe the experimental setup for anion production and ZEKE spectroscopy. In Sec. III we present the ZEKE spectra of $KrBr^-$, $XeBr^-$, and $KrCl^-$, and assign the observed electronic and vibrational structure. Section IV deals with the construction of model potentials for fitting the vibrational structure and rotational contours of the ZEKE spectra. Finally, we compare our potentials with other experimental and theoretical results in Sec. V.

II. EXPERIMENT

ZEKE spectroscopy was originally developed by Müller-Dethlefs *et al.* for photoionization of neutrals.[22–24] It was first applied to the study of anions by Neumark and co-workers.[25] The anion ZEKE apparatus used here has been described in detail elsewhere.[26–28] A brief description follows.

$KrBr^-$ and $XeBr^-$ anions are produced by expanding a mixture of 0.2% CF_2ClBr/10%–30% Kr (or Xe)/balance He into vacuum through a 0.5 mm aperture in a pulsed valve (General Valve Corp.). The expansion is crossed near the pulsed valve with a 1 keV electron beam produced with a thoria-coated iridium filament (Electron Technology). Halide anions are produced by dissociative attachment and other secondary processes, and clusters form as the supersonic expansion cools. $KrCl^-$ anions are produced by passing the Kr/He mixture over a reservoir containing CCl_4 at room temperature. Backing pressures were typically 20–80 psi.

The anions pass through a skimmer into a differentially pumped region and are accelerated to 1 keV into a 1 m collinear time-of-flight mass spectrometer. The $KrCl^-$ results were obtained using an additional skimmer in the source chamber placed very close to the beam valve.[29] The clusters separate according to mass, and the species of interest is irradiated with a pulse from an excimer-pumped dye laser (Lambda Physik) operating at a repetition rate of 30 Hz. After a 200–500 ns delay, the electrons are extracted coaxially with the ion beam using a pulsed electric field and detected approximately 1 m away with a microchannel plate detector. The electrons are detected in a 35–100 ns gate, so that as the laser wavelength is scanned, only electrons with nearly zero kinetic energy relative to the anion packet are detected. The resulting spectral resolution is about 1–2 cm^{-1} for atomic anions. The peaks observed in this work are somewhat broader because of unresolved rotational structure.

In order to study the $X1/2$ and $I3/2$ states, DMQ laser dye was used for KrBr and XeBr and PTP dye was used for KrCl. The laser pulse energy was about 20 mJ/pulse for KrBr and XeBr, and about 3–10 mJ/pulse for KrCl. These spectra were averaged over 1000–2000 laser shots/point. For the $II1/2$ states of KrBr and XeBr, light from Rhodamine 640 dye was frequency-doubled with a KDP crystal, yielding laser pulse energies of ~2–4 mJ/pulse. Spectra for the $II1/2$ states were averaged over about 8000 laser shots per point. In all cases, the electron signal was normalized to the ion signal and to the laser pulse energy. When using DMQ and PTP dyes, the laser wavelength was calibrated using a Fe–Ne hollow cathode lamp. An iodine cell was used to calibrate the fundamental wavelength when Rhodamine 640 dye was frequency doubled. The spectra were smoothed with a five-point, second-order Savitzky–Golay algorithm,[30] which had a negligible effect on the relative peak intensities.

III. RESULTS

A. KrBr

The ZEKE spectra of $KrBr^-$ are shown in Fig. 1. We observe two band systems, shown in Figs. 1(a) and 1(b), separated by approximately the spin–orbit constant of Br (3685 cm^{-1}). The lower energy band system in Fig. 1(a) results from transitions to the $X1/2$ and $I3/2$ states, and the higher energy system in Fig. 1(b) is due to the $II1/2$ state.

Assignment of the vibrational and electronic features in Fig. 1 is facilitated by our earlier studies of the ArI^-, $ArBr^-$, and KrI^- spectra.[3] Specifically, the anion vibrational frequencies are expected to be considerably larger than the neutral frequencies, and this enables one to distinguish among the three types of neutral←anion vibrational transitions ($v'-v''$) that contribute to the spectra: vibrational progressions in the neutral originating from a single anion vibrational level v'', $\Delta v=0$ sequence band transitions from a series of vibrational levels of the anion, and $\Delta v\neq 0$ hot band transitions from vibrationally excited anion levels.

Figure 1(a) is dominated by one peak, labeled **1**, with a set of smaller peaks, a_1, b_1, and c_1, spaced by about 15 cm^{-1} toward lower energy. A second, weaker progression is seen at higher energies than peak **1** with a characteristic peak spacing of 20 cm^{-1}. We assign peak **1** to the origin (0–0) transition from the anion to the $X1/2$ state. Peaks a_1, b_1, and

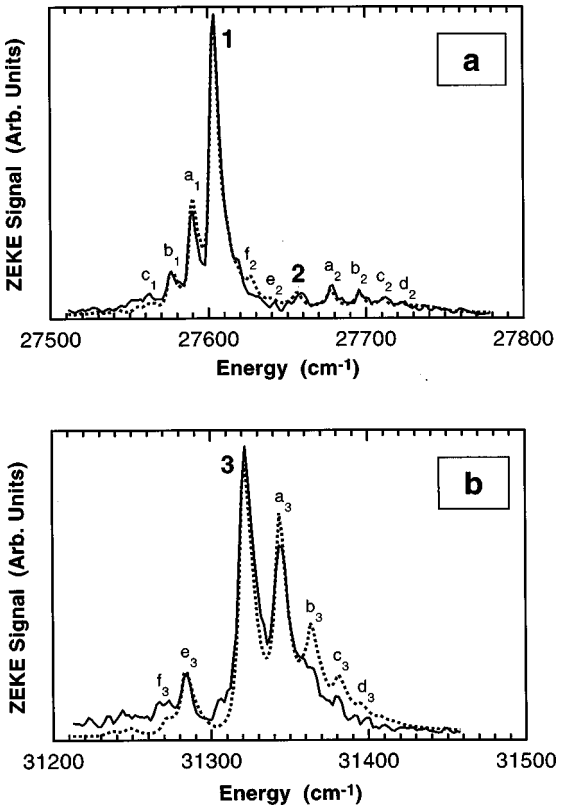

FIG. 1. Experimental and simulated ZEKE spectra of $KrBr^-$. The solid lines are the experimental spectra, and the dotted lines are the spectra calculated from the model potentials described in the text. (a) $X1/2$ and $I3/2$ states (halogen atom $^2P_{3/2}$ asymptote). (b) $II1/2$ state (halogen atom $^2P_{1/2}$ asymptote).

c_1 are assigned to $\Delta v=0$ sequence band transitions from vibrationally excited anion states, i.e., the 1–1, 2–2, and 3–3 transitions. The dominance of $\Delta v=0$ transitions shows that the anion geometry is very similar to the neutral $X1/2$ state geometry.

Peak **2**, the lowest energy member of the second progression, is assigned to the 0–0 transition to the $I3/2$ state. This assignment is made in part because it gives the best fit to a model potential (see Sec. IV). Peaks a_2, b_2, c_2, and d_2 are assigned to the $(v'-0)$ vibrational progression with $v'=1-4$ originating from the anion $v''=0$ level. The extent of this progression indicates that the $I3/2$ state bond length is significantly shifted from the anion geometry. Peak e_2 is assigned to the 1–1 sequence band of the $I3/2$ state. Peak f_2, 38.0 cm^{-1} to the red of peak **2** is assigned to the $I3/2$ 0–1 hot band transition, plus several overlapping bands from the $X1/2$ state.

In the $II1/2$ state spectrum, Fig. 1(b), we see the progression **3**, a_3, b_3, c_3, and d_3, with a characteristic spacing of about 20 cm^{-1}, and a smaller peak, e_3, 37.2 cm^{-1} below peak **3**. We assign peak **3** to the 0–0 transition to the $II1/2$ state, and the series a_3, b_3, c_3, d_3 to the $(v'-0)$ progression with $v'=1-4$. Peak e_3 corresponds to the 0–1 hot band transition, and gives an accurate value for the anion vibrational frequency.

The complete set of peak positions and assignments is given in Table I.

TABLE I. Peak assignments $(v'-v'')$ for $KrBr^-$ ZEKE spectra (Fig. 1). Energies are in cm^{-1}.

State	Peak	Position	Relative energy	Assignment
$X1/2$	**1**	27 602.9	0	0←0
	a_1	27 588.4	−14.5	1←1
	b_1	27 576.2	−26.7	2←2
	c_1	27 561.0	−41.9	3←3
$I3/2$	**2**	27 657.0	0	0←0
	a_2	27 678.4	21.4	1←0
	b_2	27 695.3	38.3	2←0
	c_2	27 710.7	53.7	3←0
	d_2	27 723.0	66.0	4←0
	e_2	27 641.7	−15.3	1←1
	f_2	27 619.0 (shoulder)	−38.0	0←1
$II1/2$	**3**	31 321.7	0	0←0
	a_3	31 343.5	21.8	1←0
	b_3	31 363.2	41.5	2←0
	c_3	31 380.6	58.9	3←0
	d_3	31 398.3	76.6	4←0
	e_3	31 284.5	−37.2	0←1
	f_3	31 274.7	−47.0	1←2

B. XeBr

The ZEKE spectra of $XeBr^-$ are shown in Figs. 2(a) and 2(b). Our assignment of the peaks proceeds in a fashion similar to the assignment of the KrBr spectrum. Again there are

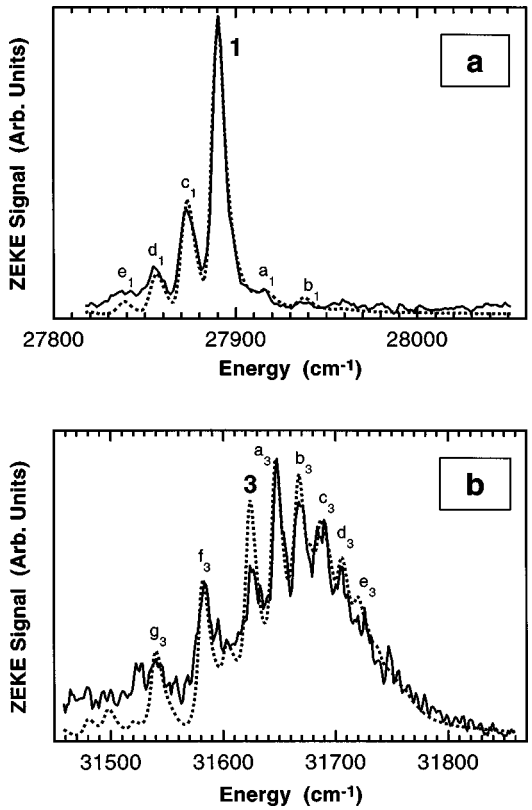

FIG. 2. Experimental and simulated ZEKE spectra of $XeBr^-$. The solid lines are the experimental spectra, and the dotted lines are the spectra calculated from the model potentials described in the text. (a) $X1/2$ state (halogen atom $^2P_{3/2}$ asymptote). The $I3/2$ state cannot be seen. (b) $II1/2$ state (halogen atom $^2P_{1/2}$ asymptote).

TABLE II. Peak assignments for $XeBr^-$ ZEKE spectra (Fig. 2). Energies are in cm^{-1}.

State	Peak	Position	Relative energy	Assignment
	1	27 890.0	0	0←0
	a_1	27 916.5	26.5	1←0
$X1/2$	b_1	27 940.2	50.2	2←0
	c_1	27 873.0	−17.0	1←1
	d_1	27 855.1	−34.9	2←2
	e_1	27 841.9	−48.1	3←3
	3	31 623.6	0	0←0
	a_3	31 647.6	24.0	1←0
	b_3	31 667.1	43.5	2←0
$II1/2$	c_3	31 687.5	63.9	3←0
	d_3	31 704.7	81.1	4←0
	e_3	31 719.8	96.2	5←0
	f_3	31 583.2	−40.4	0←1
	g_3	31 539.8	−83.8	0←2

two band systems separated approximately by the Br spin–orbit constant. The lower energy system in Fig. 2(a) is dominated by a single peak, **1**, with a set of peaks c_1, d_1, and e_1 spaced at ~17 cm^{-1} intervals toward lower energy. We also observe a pair of small peaks, a_1 and b_1, 26.5 and 50.2 cm^{-1} to the blue of peak **1**, respectively. As above we assign peak **1** to the origin transition to the $X1/2$ state, and the peaks c_1, d_1, and e_1 to the sequence bands 1–1, 2–2, and 3–3, respectively. Peaks a_1 and b_1 correspond to the 1–0 and 2–0 transitions, and are consistent within 2.5 cm^{-1} with the peak spacings calculated from the spectroscopic constants determined by Tellinghuisen and co-workers in their excimer emission study.[17] As above, the dominance of the 0–0 transition shows that the anion bond length is apparently quite close to that of the $X1/2$ state. However, in contrast to the $KrBr^-$ spectrum, transitions to the $I3/2$ state are not seen in Fig. 2(a).

The more congested $II1/2$ state spectrum in Fig. 2(b) reveals two vibrational progressions. Peaks **3**, a_3, b_3, c_3, d_3, and e_3 are spaced by 20 cm^{-1} toward higher energy, peaks **3**, f_3, and g_3 are spaced by about 42 cm^{-1} toward lower energy. Based on this change in peak spacing, peaks **3**–e_3 are assigned to a progression arising from the ground anion vibrational state with the origin at peak **3**. Peaks f_3 and g_3 are assigned to the 0–1 and 0–2 hot band transitions, respectively.

The $XeBr^-$ peak positions and assignments are given in Table II.

C. KrCl

The ZEKE spectrum of $KrCl^-$ is shown in Fig. 3. The largest peak, labeled **1**, is assigned to the origin transition to the $X1/2$ state. Peaks **1**, c_1, d_1, e_1, and f_1 are spaced approximately 26 cm^{-1} toward lower energy. The latter four peaks are assigned to $\Delta v=0$ sequence band transitions, with additional contributions from the hot band transitions listed in Table III. Also, peaks g_1 and h_1 can be assigned to the overlapping hot band transitions given in Table III. The partially resolved peaks a_1 and b_1 to the blue of peak **1** are assigned to the $(v'-0)$ progression, yielding a frequency of 29 cm^{-1} for the $X1/2$ state. We were not able to observe the $I3/2$ state or the $II1/2$ state for this system. The peak positions and assignments are shown in Table III.

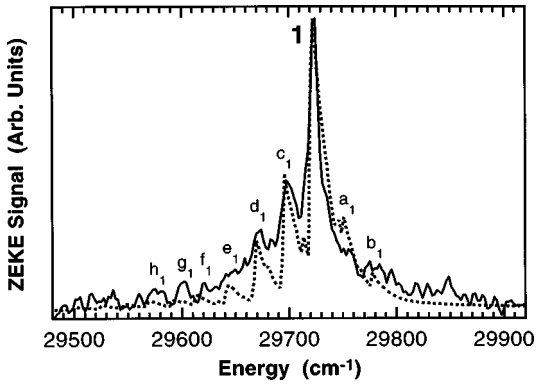

FIG. 3. Experimental and simulated ZEKE spectrum of the $X1/2$ state (halogen atom $^2P_{3/2}$ asymptote) of $KrCl^-$. The solid line is the experimental spectrum, and the dotted line is the spectrum calculated from the model potentials described in the text.

IV. ANALYSIS

For each of the three species, the energy of peak **1** yields an accurate electron affinity: 27 603(3) cm^{-1} for KrBr, 27 890(3) for XeBr, and 29 725(5) cm^{-1} for KrCl. These values are larger than the corresponding electron affinities of Br and Cl, which are 27 129.170 and 29 138.3 cm^{-1}, respectively.[31,32] The larger electron affinities for the complexes show that the RgX^- dissociation energies are greater than the RgX dissociation energies, and that $XeBr^-$ is more strongly bound than $KrBr^-$. Also, from the vibrational assignments in Tables I–III we directly obtain vibrational frequencies for the anion and neutral states.

To gain further insight into these complexes, we construct model potentials for the anion and neutral RgX complexes to simulate the experimental ZEKE spectra. The spec-

TABLE III. Peak assignments for $KrCl^-$ ZEKE spectrum (Fig. 3). Energies are in cm^{-1}. Assignments in parentheses contribute less than 20% of the total peak intensity. The assignment listed first contributes the most peak intensity.

State	Peak	Position	Relative energy	Assignment
	1	29 724.5	0	0← 0
				(2←1)
	a_1	29 753.3	28.8	1← 0
				3← 1
	b_1	29 784.2	59.7	2← 0
	c_1	29 698.1	−26.4	1← 1
				(5←3)
				(3←2)
$X1/2$	d_1	29 673.9	−50.6	2← 2
				(0←1)
	e_1	29 645.4	−79.1	3← 3
	f_1	29 621.3	−103.2	4← 4
				0← 2
	g_1	29 601.6	−122.9	1← 3
				3← 4
	h_1	29 575.4	−149.1	2← 4
				4← 5

tra are fit by choosing model anion and neutral potentials, and calculating the Franck–Condon factors, which, assuming a Boltzmann distribution for the anion vibrational population, are used to produce a simulated spectrum to be compared with the experimental spectrum. The potential parameters and vibrational temperature are then adjusted in a trial-and-error fashion to produce the best agreement between the experimental and simulated spectra. The vibrational eigenvalues are calculated from the potentials using a discrete variable representation procedure[33] based on a basis set of Morse potential eigenfunctions.[34]

We use the flexible, piecewise Morse–Morse-switching function-van der Waals (MMSV) potential form. This is the same potential form used by Lee and co-workers for the RgX neutral potentials[18] and in our previous work.[3] For the neutral, this potential has the reduced form, with $f(x)=V(R)/\epsilon$ and $x=R/R_m$:

$$f(x)=\begin{cases} e^{2\beta_1(1-x)}-2e^{\beta_1(1-x)}, & 0<x\leqslant 1 \\ e^{2\beta_2(1-x)}-2e^{\beta_2(1-x)}\equiv M_2(x), & 1<x\leqslant x_1 \\ SW(x)M_2(x)+[1-SW(x)]W(x), & x_1<x<x_2 \\ -C_{6r}x^{-6}-C_{8r}x^{-8}\equiv W(x), & x_2\leqslant x<\infty, \end{cases} \tag{1}$$

where the switching function is given by

$$SW(x)=\frac{1}{2}\left[\cos\frac{\pi(x-x_1)}{(x_2-x_1)}+1\right] \tag{2}$$

and

$$C_{6r}=\frac{C_6}{\epsilon R_m^6},\quad C_{8r}=\frac{C_8}{\epsilon R_m^8}. \tag{3}$$

Here, ϵ is the potential well depth and R_m is the bond length. C_6 is the induced dipole-induced dipole dispersion coefficient, and C_8 represents the induced dipole-induced quadrupole dispersion coefficient. Higher dispersion terms are neglected, as is the small induction term, varying as R^{-8}, arising from the halogen permanent quadrupole moment.

The anion potentials are of the same form, except that the dispersion terms are replaced by

$$f(x)=-B_{4r}x^{-4}-B_{6r}x^{-6}\equiv W(x),\quad x_2\leqslant x<\infty \tag{4}$$

with

$$B_{4r}=\frac{B_4}{\epsilon R_m^4},\quad B_{6r}=\frac{B_6}{\epsilon R_m^6} \tag{5}$$

and

$$B_4=\frac{1}{2}q^2\alpha_d^{\mathrm{Rg}},\quad B_6=\tfrac{1}{2}q^2\alpha_q^{\mathrm{Rg}}+C_6. \tag{6}$$

Here, q is the halide charge and B_4 is the coefficient of the dominant term in the long range RgX^- potential, reflecting the dipole induced in the rare gas atom by the halide charge. The B_6 term arises from quadrupole induction and dipole dispersion terms. α_d^{Rg} and α_q^{Rg} are the dipole and quadrupole polarizabilities of the rare gas, respectively.

The dispersion coefficients C_6 and C_8 are estimated using the formulas of Koutselos *et al.*[35] These formulas involve the dipole and quadrupole polarizabilities of each interacting atom, and an effective number of electrons, N, characteristic of each atom. N is empirically determined from the like-atom C_6 coefficients.[36–38] In the case of the halide atoms, the values of N are assumed to be the same as those of the isoelectronic rare gas atoms.

In calculating the dispersion coefficients for the neutral RgX complexes one must account for the open shell nature of the halogen atoms which results in anisotropic polarizabilities. The anisotropy of the dipole polarizability has been calculated for the Cl atom, neglecting spin–orbit effects, to be 14% relative to the average over all M_L states.[39] The halogen in the Σ state of a RgX complex, with the unpaired electron oriented along the internuclear axis, has a smaller polarizability and smaller dispersion interaction than in the Π state, where the unpaired electron is perpendicular to the axis. Bartolotti *et al.*[40] have calculated the anisotropy of the quadrupole polarizability of the Cl atom. However, in this calculation the value given for the quadrupole polarizability of the Ar atom is 18% higher than the accurate value of Thakkar *et al.*[41] Therefore, the Cl quadrupole polarizabilities have been scaled down by this amount. This gives an anisotropy of 16% for α_q. Because the anisotropy of α_d of Br has not been calculated, it was assumed to be the same as that of Cl. Likewise, because calculations of α_q are not available for Br, these were estimated using the ''hydrogenic relationship'' discussed by Sastri *et al.*:[42]

$$\alpha_q\cong 1.570\alpha_d^{3/2}, \tag{7}$$

where both polarizabilities are in atomic units. The anisotropy of α_q was also assumed to be the same for Br as for Cl. To find the dispersion coefficients for states including spin–orbit effects, we note that the $I3/2$ state has pure Π character, while at long range the $X1/2$ state is a mixture of 2/3 Σ and 1/3 Π character, and the $II1/2$ state has 1/3 Σ and 2/3 Π character.[21] We assume that these mixing coefficients are constant for all regions of the potential where dispersion plays a role [i.e., $x>x_1$ in Eq. (1)].

The polarizabilities and effective numbers of electrons used here can be found in Table IV. The C_6 and C_8 coefficients for the various interactions are given with the other potential parameters, discussed below, in Tables V–VII. The C_6 values are fairly close to those of Lee and co-workers,[18] but the C_8 coefficients are in general larger because Lee and co-workers approximated C_8 with the values from the isoelectronic rare gas pairs. Because the ZEKE spectra are not sensitive to the very long range part of the potential, B_4, B_6, C_6, and C_8 were kept fixed at the calculated values during the fitting procedures.

Since the ZEKE spectra do not give information about the absolute values of ϵ and R_m, we have used results from previous experiments to guide our choice of these parameters. For KrBr, we fix R_m and ϵ of the $X1/2$ state at the values determined in the scattering experiments of Lee and co-workers.[18] For KrCl the values determined by Aquilanti and co-workers for the $X1/2$ state are used.[19] For XeBr, R_m and ϵ are taken from the $X1/2$ state potential of Tellinghuisen and co-workers,[16,17] which they obtained by combining their vibrationally resolved $B1/2\rightarrow X1/2$ emission spectrum with the repulsive wall of the potential of Lee and co-workers.[18]

TABLE IV. Dipole and quadrupole polarizabilities and effective numbers of electrons used to calculate dispersion and induction coefficients. In atomic units.

Atom	Corresponding neutral spinless state	α_d	α_q	N
Cl	Σ	13.3[a]	72.0[b]	4.2[c]
	Π	15.3[a]	84.9[b]	4.2[c]
Br	Σ	18.7[d]	131[e]	6.2[c]
	Π	21.5[d]	154[e]	6.2[c]
Cl^-	⋯	28.1[c]	⋯	5.404[f]
Br^-	⋯	36.4[c]	⋯	6.309[f]
Kr	⋯	16.79[g]	99.296[h]	6.309[i]
Xe	⋯	27.16[g]	223.29[h]	7.253[i]

[a]Reference 39.
[b]Values from Ref. 40, scaled by a factor of 0.822 as explained in the text.
[c]Reference 36.
[d]Derived from the spherically averaged value given in Ref. 36, assuming the same anisotropy for Br as for Cl.
[e]Calculated from α_d of Br using the ''hydrogenic relationship'' $\alpha_q \cong 1.570\ \alpha_d^{3/2}$ given in Ref. 42.
[f]Calculated from the C_6 values of the corresponding isoelectronic rare gases from Ref. 37, using the Slater–Kirkwood formula (see, e.g., Ref. 38).
[g]Reference 37.
[h]Reference 41.
[i]Calculated from the C_6 values from Ref. 37.

The emission spectrum independently provides a more precise well depth ϵ than could be determined from the scattering experiments alone: Clevenger and Tellinghuisen cite an uncertainty of 0.8% for their value of ϵ, significantly more precise than the uncertainty cited for the scattering results (~5%). However, the uncertainty in R_m is essentially the same as in Lee's potential (~10%).

To determine ϵ for the anions and the remaining electronic states we then use the relationships implied by Fig. 4, namely:

$$\epsilon_{\rm an} = \nu_{00}(X1/2) + \omega_0^{\rm an} + \epsilon_X - \omega_0^X - {\rm EA}, \tag{8}$$

$$\epsilon_I = \epsilon_X - \Delta_{X-I} - \omega_0^X + \omega_0^I, \tag{9}$$

$$\epsilon_{II} = \epsilon_X + \Delta_{\rm so} - \Delta_{X-II} - \omega_0^X + \omega_0^{II}, \tag{10}$$

where $\nu_{00}(X1/2)$ is the origin of the $X1/2$ state, $\omega_0^{\rm an}$, ω_0^X, etc., represent zero point energies, EA is the electron affinity of the halogen atom, Δ_{X-I} is the $X1/2$–$I3/2$ state splitting (between $v=0$ levels), and Δ_{X-II} is the $X1/2$–$II1/2$ state splitting.

Once ϵ is fixed for the $I3/2$, $II1/2$ and anion states, R_m is found for these potentials by first adjusting R_m of the anion to best reproduce the observed peak intensities of the $X1/2$ state portion of the spectrum. When R_m is known for the anion, R_m for the $I3/2$ and $II1/2$ states can then also be found by means of the Franck–Condon simulation.

For KrBr the initial values of the $X1/2$ and $I3/2$ state potential parameters β_1, β_2, x_1, and x_2 were taken to be the same as Lee's values.[18] The β_1 parameter was kept fixed at the initial value because of the observation by Lee and coworkers that the slope of the repulsive part of the potential, with this β_1 value, agrees well with the slope determined from analysis of the excimer emission.[18] The remaining parameters, β_2, x_1, and x_2 were then adjusted to reproduce the peak spacings seen in the ZEKE spectra.

In the case of XeBr, the β_1, β_2, x_1, and x_2 parameters of the $X1/2$ state were adjusted to best fit the Rydberg–Klein–Rees (RKR) turning points determined by Tellinghuisen and co-workers.[17] With this potential form, it was possible to reproduce the RKR turning point energies to within 3.5 cm^{-1}. The vibrational spacings for the first nine levels of the resulting MMSV potential are within 0.2 cm^{-1} of those calculated from Tellinghuisen's spectroscopic constants, with the exception of the $v=0$ to $v=1$ spacing, which differed by 0.4 cm^{-1}. This level of agreement was judged to be sufficient for the purposes of this work. Because of the accuracy of the Tellinghuisen potential, no adjustments were made to the $X1/2$ state MMSV parameters during the fitting procedure.

For KrCl, the shape of the $X1/2$ state potential was estimated by choosing the MMSV parameters to reproduce the

TABLE V. MMSV potential parameters for KrBr and $KrBr^-$, and zero point energies (ω_0) and fundamental vibrational frequencies (ν_{01}) calculated from the potentials. Term values T_0 are referenced to anion ground vibrational state. Estimated uncertainties are given in parentheses.

	$X1/2$	$I3/2$	$II1/2$	Anion
$T_{\rm vib}$ (K) of anion	68.0 (4.0)	68.0 (4.0)	45.0 (3.0)	⋯
T_0 (cm^{-1})	27 602.9 (2.0)	27 657.0 (4.0)	31 321.7 (2.0)	0
ω_0 (cm^{-1})	12.5	11.7	12.4	19.2
ν_{01} (cm^{-1})	23.8	21.4	22.8	37.2
ϵ (meV)	19.9 (1.0)	13.1 (0.9)	15.7 (1.0)	79.5 (1.0)
R_m (Å)	3.90 (0.30)	4.15 (0.30)	4.03 (0.30)	3.85 (0.30)
β_1	5.70 (0.40)	7.20 (0.50)	7.00 (0.50)	4.62 (0.30)
β_2	6.72 (0.30)	8.00 (0.30)	7.20 (0.30)	4.62 (0.20)
x_1	1.02 (0.06)	1.05 (0.06)	1.05 (0.06)	1.04 (0.06)
x_2	1.70 (0.20)	1.65 (0.10)	1.85 (0.20)	1.50 (0.10)
C_6 (eV $Å^6$)	86.6 (13.0)	92.7 (14.0)	89.6 (13.0)	⋯
C_8 (eV $Å^8$)	740.0 (220.0)	801.0 (240.0)	771.0 (230.0)	⋯
B_4 (eV $Å^4$)	⋯	⋯	⋯	17.91 (2.70)
B_6 (eV $Å^6$)	⋯	⋯	⋯	165.0 (41.0)

TABLE VI. MMSV potential parameters for XeBr and $XeBr^-$, and zero point energies (ω_0) and fundamental vibrational frequencies (ν_{01}) calculated from the potentials. Term values T_0 are referenced to anion ground vibrational state. Estimated uncertainties are given in parentheses.

	$X1/2$	$II1/2$	Anion
T_{vib} (K) of anion	70.0 (4.0)	90.0 (5.0)	⋯
T_0 (cm^{-1})	27 890.0 (2.0)	31 623.6 (4.0)	0
ω_0 (cm^{-1})	12.3	12.6	21.3
ν_{01} (cm^{-1})	24.1	23.1	42.1
ϵ (meV)	31.53 (0.25)	25.52 (0.74)	126.92 (0.50)
R_m (Å)	3.82 (0.19)	4.00 (0.22)	3.81 (0.21)
β_1	4.35 (0.30)	6.42 (0.45)	3.50 (0.25)
β_2	7.41 (0.30)	7.00 (0.28)	5.30 (0.21)
x_1	1.01 (0.06)	1.03 (0.06)	1.03 (0.06)
x_2	2.00 (0.24)	1.60 (0.19)	1.60 (0.19)
C_6 (eV $Å^6$)	129.0 (19.0)	133.0 (20.0)	⋯
C_8 (eV $Å^8$)	1270.0 (380.0)	1320.0 (400.0)	⋯
B_4 (eV $Å^4$)	⋯	⋯	28.98 (4.30)
B_6 (eV $Å^6$)	⋯	⋯	271.0 (68.0)

TABLE VII. MMSV potential parameters for KrCl and $KrCl^-$, and zero point energies (ω_0) and fundamental vibrational frequencies (ν_{01}) calculated from the potentials. Term values T_0 are referenced to anion ground vibrational state. Estimated uncertainties are given in parentheses.

	$X1/2$	Anion
T_{vib} (K) of anion	210.0 (10.0)	⋯
T_0 (cm^{-1})	29 724.5 (2.0)	0
ω_0 (cm^{-1})	16.0	29.3
ν_{01} (cm^{-1})	29.9	55.5
ϵ (meV)	22.01 (1.00)	95.7 (1.0)
R_m (Å)	3.75 (0.10)	3.83 (0.10)
β_1	5.49 (0.40)	5.70 (0.50)
β_2	5.70 (0.20)	4.40 (0.20)
x_1	1.30 (0.08)	1.30 (0.06)
x_2	1.90 (0.20)	2.50 (0.20)
C_6 (eV $Å^6$)	60.8 (9.1)	⋯
C_8 (eV $Å^8$)	473.0 (71.0)	⋯
B_4 (eV $Å^4$)	⋯	17.91 (2.70)
B_6 (eV $Å^6$)	⋯	138.0 (35.0)

$X1/2$ state potential of Aquilanti and co-workers,[19] who used a different representation of the potentials. This was not modified during the fitting because of the absence of sufficient detail in the ZEKE spectrum. Therefore, in the KrCl simulation only the anion parameters are adjusted.

Once the potentials are established by the Franck–Condon fitting procedure, a rotational simulation is performed to fit the observed asymmetric peak shapes. In this procedure, a set of rotational lines are calculated for each vibrational band, and these are convoluted with the asymmetric ZEKE instrumental line shape. The intensity of the ZEKE electron signal, $I(E)$, due to an individual line is represented by

$$I(E)=\begin{cases} \dfrac{a\left(\dfrac{E-E_0}{\Gamma}\right)+b\left(\dfrac{E-E_0}{\Gamma}\right)^3}{1+c\left(\dfrac{E-E_0}{\Gamma}\right)^2+d\left(\dfrac{E-E_0}{\Gamma}\right)^4}, & E\geqslant E_0 \\ 0, & E<E_0 \end{cases} \tag{11}$$

with $a=4.3$, $b=0.19$, $c=4.2$, and $d=2.3$, and where $E-E_0$ is the energy above the threshold, E_0, of the line in cm^{-1}, and Γ is the full width at half-maximum (FWHM) in cm^{-1}. The line shape parameters are obtained by a nonlinear least-squares fit to the ZEKE spectra of Br^-. This form differs from that used previously[3] and is a more accurate representation of the true ZEKE line shape. Readers are referred to our previous work[3] for further details of the rotational fitting procedure. As in previous work, the rotational temperature was assumed to be 40 K.

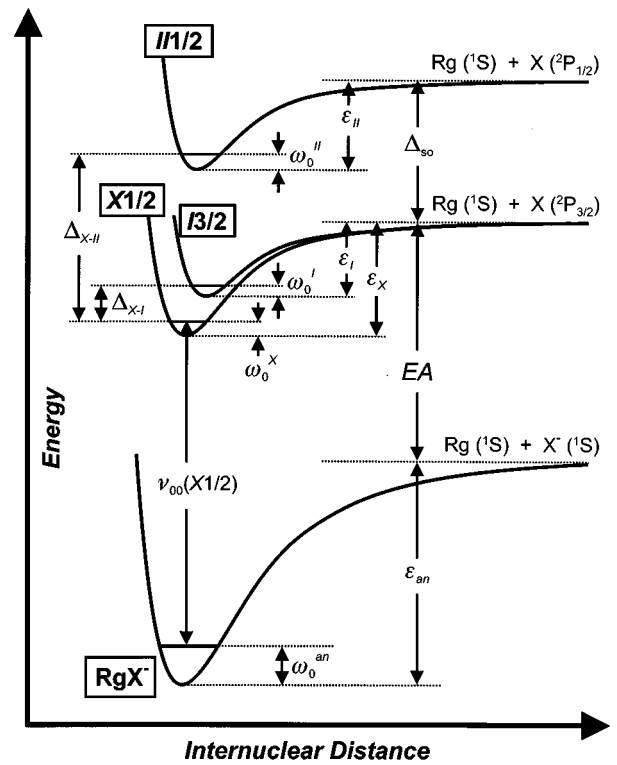

FIG. 4. Schematic potential energy level diagram, showing the energetic relations among the atomic and molecular anion and neutral electronic states.

The simulated spectra are shown as dotted lines superimposed on the experimental spectra in Figs. 1–3. The best-fit potential parameters are given in Tables V–VII, and the potentials are plotted in Fig. 5. For the $KrBr^-$ and $XeBr^-$ spectra, the anion vibrational temperature for the $II1/2$ state differs slightly from the lower energy state(s) because the spectra were taken with different source conditions.

Fitting the XeBr and KrCl spectra is fairly straightforward, because the peak assignments are readily apparent by inspection of the spectra. However, for KrBr the fitting procedure is used as an aid in assigning spectral features, since not all of the assignments are obvious from the spectra. Specifically, although the assignments of the $X1/2$ state features are straightforward, the location of the origin of the $I3/2$ state is not obvious upon initial inspection. As mentioned in Sec. III A, peak **2** of Fig. 1(a) is assigned to the $I3/2$ origin because this allows the best fit with the model potential. Also, this assignment gives a value of the $X1/2-I3/2$ state split-

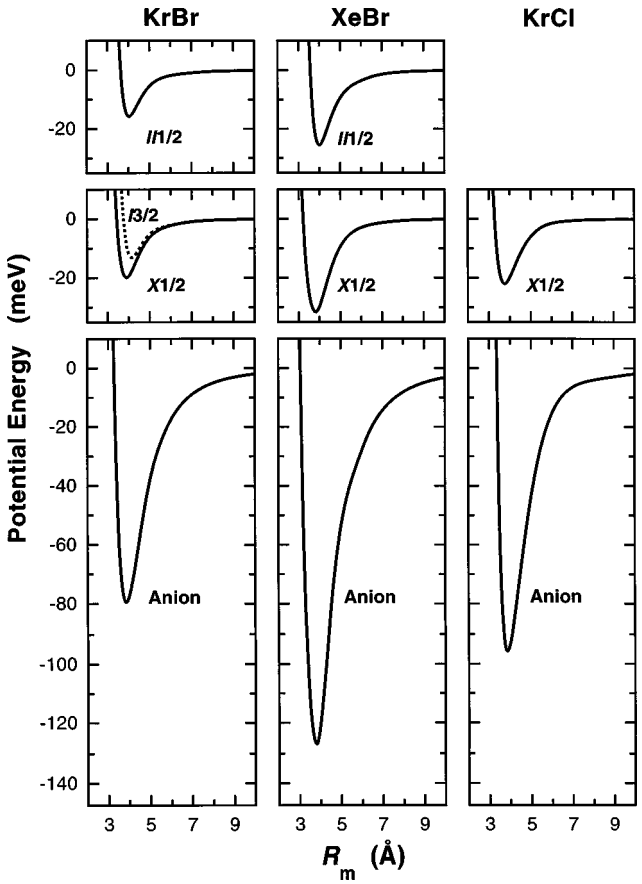

FIG. 5. Plots of model potentials for the RgX anion and observed neutral states determined from the ZEKE spectra, using the MMSV potential parameters given in Tables V–VII.

ting, Δ_{X-I}, of 54.1 cm^{-1}. This is somewhat larger than Δ_{X-I} for ArBr, 37.8 cm^{-1},[3] a result expected due to the stronger Kr–Br interaction. On the other hand, if peak e_2 were chosen as the $I3/2$ state origin, Δ_{X-I} would essentially be the same as in ArBr, contrary to expectation. This further corroborates our choice of peak **2** as the $I3/2$ state origin.

The method for estimating the uncertainties of the potential parameters is discussed at length in our earlier work.[3] Here, we present these estimated uncertainties along with the potential parameters in Tables V–VII. The anion and neutral potentials are plotted in Fig. 5. It should be remembered that the uncertainties in ϵ and R_m are expected to be fairly rigorous, whereas the uncertainties given for the other potential parameters represent lower bounds on the true uncertainties, because a complete multivariate analysis of the correlations among these parameters was not performed.

V. DISCUSSION

In this section we discuss our results for the neutral and anion RgX potentials and compare them to previously published potentials. The neutral potentials presented here do not differ greatly from earlier potentials. For the KrBr $X1/2$ state, of course, ϵ and R_m are the same as those from Lee's study,[18] because these were not adjusted in our fitting procedure. Our values of β_2, x_1, and x_2 differ somewhat from Lee's values and result in an improved match with the vibrational spacings in the ZEKE spectra. As mentioned above, β_1 was not adjusted, in order to retain agreement with the repulsive wall slope from emission studies. For the $I3/2$ state of KrBr, the bond length is somewhat longer and the well depth a bit shallower than Lee's values. The difference in R_m values is well within the stated 10% uncertainty, but the difference in ϵ is just outside this range at 12%.

Our XeBr $X1/2$ state potential is more or less identical with that determined by Clevenger and Tellinghuisen,[17] differing only because of the limitations of the MMSV potential form, and was not varied during the fit because of the much higher relative accuracy of the emission results. The few features of the XeBr $X1/2$ state observed in the ZEKE spectrum (the progression $v'=0,1,2 \leftarrow v''=0$, i.e., peaks **1**, a_1, and b_1 in Fig. 2) are consistent with the emission results within our experimental uncertainty.

Our $X1/2$ state potential for KrCl is essentially identical to the integral cross-section potential,[19] differing only in the choice of potential form. This is because the ZEKE spectra do not contain enough information to significantly improve on the potential obtained from the scattering experiments.

We obtain significantly more new information about the anion potentials. The trends in anion binding energies are similar to those seen in our previous study.[3] The larger binding energy for $XeBr^-$ compared to $KrBr^-$ is due to the larger polarizability of Xe, and the larger binding energy of $KrCl^-$ vs $KrBr^-$ results from the smaller R_m and stronger charge-polarizability attraction in $KrCl^-$. For all three anions, the change in R_m upon photodetachment to the $X1/2$ state is very small, even though the anion binding energy is considerably larger. Apparently the larger radius of the halide in the anions compensates for the stronger binding energy.

In Table VIII, we compare the potential parameters R_m and ϵ of the anions from the present study with other values from the literature, all of which have been derived through less direct means. It can be seen that the literature values are quite scattered. In comparing our results with the results of Kirkpatrick and Viehland,[7] who obtained potentials via direct inversion of ion mobility data, we find our well depths are systematically shallower and our bond lengths systematically longer. However, except for the $XeBr^-$ well depth, our values lie within or close to the 10% uncertainties cited by those authors. Similar discrepancies with other ZEKE potentials were explored in a recent paper by Kirkpatrick and Viehland, in which they used the ZEKE potentials[3] of ArI^- and $ArBr^-$ to simulate ion mobilities.[43] They found that the ZEKE ArI^- potential satisfactorily reproduced the mobility data, despite significant differences in R_m and ϵ from the potentials obtained by direct inversion of mobility data. However, the agreement for $ArBr^-$ was not as good. The authors cite the relative insensitivity of the mobility data to well depth to explain these findings.

Potentials derived from the earlier mobility results of McDaniel and co-workers[6] for $KrBr^-$ and $XeBr^-$ are slightly closer to ours, but show the same sign and order of magnitude deviations in ϵ and R_m. The electron gas calculations of Waldman and Gordon[9] again give systematically larger well depths than ours, although the bond lengths are in reasonable agreement. The recent *ab initio* calculation by Schröder

TABLE VIII. Comparison of ZEKE-determined anion potentials with literature potentials. Uncertainties are given in parentheses as reported in each work cited, if available.

	$KrBr^-$		$XeBr^-$		$KrCl^-$	
	ϵ (meV)	R_m (Å)	ϵ (meV)	R_m (Å)	ϵ (meV)	R_m (Å)
Present work	79.5 (1.0)	3.85 (0.30)	126.92 (0.50)	3.81 (0.21)	95.7 (1.0)	3.83 (0.10)
Ion mobilities[a]	87.1	3.73	145	3.62	⋯	⋯
Ion mobilities[b]	88.7 (8.9)	3.579	169 (17)	3.397	102 (10)	3.448
Electron gas[c]	93	3.76	159	3.64	⋯	⋯
Electron gas[d]	⋯	⋯	⋯	⋯	115	3.48
Empirical[e]	98	3.99	142	4.10	105	3.85
Empirical[f]	90.1	3.91	130	4.02	95.4	3.79
Semiempirical[g]	92.5	3.70	167	3.62	107	3.55
Semiempirical[h]	75.1	3.87	99.9	4.05	⋯	⋯
Semiempirical[i]	85	3.79	146	3.74	108	3.53
Ab initio[j]	⋯	⋯	104	4.01	⋯	⋯

[a]Reference 6.
[b]Reference 7.
[c]Reference 9.
[d]Reference 8.
[e]Reference 12.
[f]Empirical method of Ref. 12 modified as explained in the text.
[g]Reference 35.
[h]Reference 10.
[i]Reference 11.
[j]Reference 14.

et al.[14] yields a shallow potential with a longer bond length than is found experimentally.

The results of Pirani and co-workers in Table VIII are obtained by very simple formulas based on empirical polarizability correlations.[12] Comparison to the ZEKE potentials show discrepancies greater than our experimental uncertainties, except for R_m of $KrBr^-$ and $KrCl^-$. Because of the simplicity of this method, and its usefulness for predicting new potentials, it is of interest to ''recalibrate'' these polarizability correlation formulas using the current and earlier ZEKE results. Fitting the ϵ and R_m parameters of the current study, and also those of the previous work on KrI^-, $ArBr^-$, and ArI^- we obtain

$$R_m = 1.725 \frac{\alpha_I^{1/3} + \alpha_B^{1/3}}{\left[\alpha_I \alpha_B \left(1 + \frac{1}{\rho}\right)\right]^{0.095}} \text{ Å} \tag{12}$$

and

$$\epsilon = 4380 \frac{\alpha_B}{R_m^4} (1 + \rho) \text{ meV} \tag{13}$$

with

$$\rho = \frac{\alpha_I \alpha_B}{[1 + (2\alpha_I/\alpha_B)^{2/3}]\alpha_B^{3/2}}. \tag{14}$$

Here the anion and neutral polarizabilities, α_I and α_B, are in $Å^3$ and R_m is in Å. The numerical coefficients in Eqs. (12) and (13) differ somewhat from Pirani's values, 1.767 and 5200,[12] which were obtained using ϵ and R_m for the Li^+–He and Li^+–Ne interaction potentials as references. The results using our parameters are given in Table VIII; a significant improvement is obtained, although agreement is certainly not perfect. Equations (12) and (13) should be useful in predicting other halide–rare gas interactions; this will be tested in ongoing studies of similar species.

Recent simulations by Zeiri[5] on Xe_nBr and Xe_nBr^- clusters predict that anion photodetachment will lead to rapid fragmentation of the neutral cluster, because photodetachment accesses the repulsive wall of the XeBr potential. However, these simulations use the parameters of Kirkpatrick and Viehland[7] for $XeBr^-$ and a XeBr potential with a longer R_m than that given in Table VI. This results in a very large increase in the equilibrium bond length upon photodetachment, 0.770 Å, whereas our potentials indicate that the neutral $X1/2$ state and anion have essentially identical bond lengths. The use of more accurate pair potentials should therefore have a significant effect on this aspect of the cluster simulations.

Finally, we should remark on the apparent absence of the $I3/2$ state in the $XeBr^-$ and $KrCl^-$ ZEKE spectra, and the much lower intensity of this state relative to the $X1/2$ state in the $KrBr^-$ ZEKE spectrum. Examination of these and our previous results on ArI^-, $ArBr^-$, and KrI^- shows an overall trend in which the $I3/2$ transition is weaker for smaller halides and larger rare gas atoms. Such an effect can arise if the overall photodetachment transition dipole to the $I3/2$ state is smaller. Alternatively, since the ZEKE experiment is only sensitive to those photoelectrons ejected with orbital angular momentum $l=0$,[25] the diminished intensity of the $I3/2$ state could result if the *s*-wave partial detachment cross section near threshold were smaller than for the $X1/2$ state. Preliminary results[44] in which the photoelectron spectrum and ZEKE spectrum of XeI^- are compared indicate that the transition moments to the two XeI states are similar, and that the *s*-wave partial cross section is smaller for near threshold detachment to the $I3/2$ state of XeI.

VI. CONCLUDING REMARKS

In this article, we have presented the ZEKE spectra of the RgX^- complexes $KrBr^-$, $XeBr^-$, and $KrCl^-$. We have obtained accurate electron affinities for these systems. Model anion and neutral potentials were constructed by Franck–Condon simulations of the spectra. In cases where comparison is possible, the neutral potentials are in reasonable agreement with the potentials from scattering experiments, with some minor adjustments in the well region for KrBr and XeBr. The anion potentials constructed from the data are, we believe, the most accurate experimental determinations available for these systems so far.

We have recently obtained results for Ar_nCl^- and Xe_nI^- clusters. Analysis of these spectra will yield further insight into the pair potentials and many-body interactions that govern bonding and structure in these species.

ACKNOWLEDGMENTS

This research is supported by the Air Force Office of Scientific Research under Grant No. F49620-97-1-0018. G.R. and T.L. thank the Deutsche Forschungsgemeinschaft for postdoctoral fellowships.

[1] G. C. Maitland, M. Rigby, E. B. Smith, and W. A. Wakeham, *Intermolecular Forces* (Oxford University Press, Oxford, 1981).
[2] R. A. Aziz, in *Inert Gases*, edited by M. L. Klein (Springer, Berlin, 1984), p. 5.
[3] Y. Zhao, I. Yourshaw, G. Reiser, C. C. Arnold, and D. M. Neumark, J. Chem. Phys. **101**, 6538 (1994).
[4] I. Yourshaw, Y. Zhao, and D. M. Neumark, J. Chem. Phys. **105**, 351 (1996).
[5] Y. Zeiri, J. Phys. Chem. A **102**, 2785 (1998).
[6] D. R. Lamm *et al.*, J. Chem. Phys. **79**, 1965 (1983).
[7] C. C. Kirkpatrick and L. A. Viehland, Chem. Phys. **98**, 221 (1985).
[8] Y. S. Kim and R. G. Gordon, J. Chem. Phys. **61**, 1 (1974).
[9] M. Waldman and R. G. Gordon, J. Chem. Phys. **71**, 1325 (1979).
[10] J. W. Wilson, J. H. Heinbockel, and R. A. Outlaw, J. Chem. Phys. **89**, 929 (1988).
[11] S. H. Patil, J. Chem. Phys. **89**, 6357 (1988).
[12] D. Cappelletti, G. Liuti, and F. Pirani, Chem. Phys. Lett. **183**, 297 (1991).
[13] E. J. Mansky and M. R. Flannery, J. Chem. Phys. **99**, 1962 (1993).
[14] D. Schröder, J. N. Harvey, M. Aschi, and H. Schwarz, J. Chem. Phys. **108**, 8446 (1998).
[15] P. J. Hay, W. R. Wadt, and T. H. Dunning, Jr., Annu. Rev. Phys. Chem. **30**, 311 (1979).
[16] J. O. Clevenger and J. Tellinghuisen, Chem. Phys. Lett. **231**, 515 (1994).
[17] J. O. Clevenger and J. Tellinghuisen, J. Chem. Phys. **103**, 9611 (1995).
[18] P. Casavecchia, G. He, R. K. Sparks, and Y. T. Lee, J. Chem. Phys. **75**, 710 (1981).
[19] V. Aquilanti, D. Cappelletti, V. Lorent, E. Luzzatti, and F. Pirani, J. Phys. Chem. **97**, 2063 (1993).
[20] V. Aquilanti, G. Liuti, F. Pirani, and F. Vecchiocattivi, J. Chem. Soc., Faraday Trans. 2 **85**, 955 (1989).
[21] H. Haberland, Z. Phys. A **307**, 35 (1982).
[22] K. Müller-Dethlefs, M. Sander, and E. W. Schlag, Z. Naturforsch. Teil A **39**, 1089 (1984).
[23] K. Müller-Dethlefs, M. Sander, and E. W. Schlag, Chem. Phys. Lett. **12**, 291 (1984).
[24] K. Müller-Dethlefs and E. W. Schlag, Annu. Rev. Phys. Chem. **42**, 109 (1991).
[25] T. N. Kitsopoulos, I. M. Waller, J. G. Loeser, and D. M. Neumark, Chem. Phys. Lett. **159**, 300 (1989).
[26] C. C. Arnold, Y. Zhao, T. N. Kitsopoulos, and D. M. Neumark, J. Chem. Phys. **97**, 6121 (1992).
[27] T. N. Kitsopoulos, Ph.D. thesis, University of California, 1991.
[28] C. C. Arnold, Ph.D. thesis, University of California, 1994.
[29] I. Yourshaw, T. Lenzer, and D. M. Neumark (unpublished).
[30] W. H. Press, S. A. Teukolsky, W. T. Vetterling, and B. P. Flannery, *Numerical Recipes*, 2nd ed. (Cambridge University Press, Cambridge, 1992).
[31] C. Blondel, P. Cacciani, C. Delsart, and R. Trainham, Phys. Rev. A **40**, 3698 (1989).
[32] R. Trainham, G. D. Fletcher, and D. J. Larson, J. Phys. B **20**, L777 (1987).
[33] J. C. Light, I. P. Hamilton, and J. V. Lill, J. Chem. Phys. **82**, 1400 (1985).
[34] E. M. Greenawalt and A. S. Dickinson, J. Mol. Spectrosc. **30**, 427 (1969).
[35] A. D. Koutselos, E. A. Mason, and L. A. Viehland, J. Chem. Phys. **93**, 7125 (1990).
[36] E. A. Mason and E. W. McDaniel, *Transport Properties of Ions in Gases* (Wiley, New York, 1988).
[37] A. Kumar and W. J. Meath, Mol. Phys. **54**, 823 (1985).
[38] J. N. Wilson, J. Chem. Phys. **43**, 2564 (1965).
[39] K. Andersson and A. J. Sadlej, Phys. Rev. A **46**, 2356 (1992).
[40] L. J. Bartolotti, L. Ortiz, and Q. Xie, Int. J. Quantum Chem. **49**, 449 (1994).
[41] A. J. Thakkar, H. Hettema, and P. E. S. Wormer, J. Chem. Phys. **97**, 3252 (1992).
[42] M. V. K. Sastri, P. L. Narasimhulu, and K. D. Sen, J. Chem. Phys. **80**, 584 (1984).
[43] L. A. Viehland and C. C. Kirkpatrick, Chem. Phys. **202**, 285 (1996).
[44] T. Lenzer, M. R. Furlanetto, K. R. Asmis, and D. M. Neumark, J. Chem. Phys. (submitted).